Hydrogen Peroxide-Mediated Isoniazid Activation Catalyzed by *Mycobacterium tuberculosis* Catalase−Peroxidase (KatG) and Its S315T Mutant[†,‡]

Xiangbo Zhao,[§,||] Hong Yu,[⊥] Shengwei Yu,[§] Feng Wang,[⊥] James C. Sacchettini,[⊥] and Richard S. Magliozzo*[,§,||]

Department of Chemistry, Brooklyn College, Brooklyn, New York 11210, Department of Biochemistry, The Graduate Center of the City University of New York, New York, New York 10016, and Department of Biochemistry and Biophysics, Center for Structural Biology, Texas A&M University, College Station, Texas 77843

Received September 28, 2005; Revised Manuscript Received February 14, 2006

ABSTRACT: Inhibition of the enzyme *Mycobacterium tuberculosis* InhA (enoyl-acyl carrier protein reductase) due to formation of an isonicotinoyl-NAD adduct (IN-NAD) from isoniazid (INH) and nicotinamide adenine dinucleotide cofactor is considered central to the mode of action of INH, a first-line treatment for tuberculosis infection. INH action against mycobacteria requires catalase−peroxidase (KatG) function, and IN-NAD adduct formation is catalyzed in vitro by *M. tuberculosis* KatG under a variety of conditions, yet a physiologically relevant approach to the process has not emerged that allows scrutiny of the mechanism and the origins of INH resistance in the most prevalent drug-resistant strain bearing KatG[S315T]. In this report, we describe how hydrogen peroxide, delivered at very low concentrations to ferric KatG, leads to efficient inhibition of InhA due to formation of the IN-NAD adduct. The rate of adduct formation mediated by wild-type KatG was about 20-fold greater than by the isoniazid-resistant KatG[S315T] mutant under optimal conditions (H_2O_2 supplied along with NAD^+ and INH). Slow adduct formation also occurs starting with NADH and INH, in the presence of KatG even in the absence of added peroxide, due to endogenous peroxide. The poor efficiency of the KatG[S315T] mutant can be enhanced merely by increasing the concentration of INH, consistent with this enzyme's reduced affinity for INH binding to the resting enzyme and the catalytically competent enzyme intermediate (Compound I). Origins of drug resistance in the KatG[S315T] mutant enzyme are analyzed at the structural level through examination of the three-dimensional X-ray crystal structure of the mutant enzyme.

Isoniazid has been commonly used for the treatment of tuberculosis for over 50 years (*1*, *2*). The growing appearance of INH[1]-resistant TB infections throughout the world has led to an increased interest in exploring the bactericidal function of this drug and the origins of drug resistance. We have devoted recent efforts to the examination of the structure and function of *Mycobacterium tuberculosis* catalase−peroxidase (KatG), a dual function heme enzyme demonstrated to be required for INH sensitivity (*3*, *4*), and the mutant enzyme, KatG[S315T], found in the majority of INH-resistant *M. tuberculosis* strains (*5*−*8*).

INH is a prodrug susceptible to oxidative reactions catalyzed by KatG (*9*). The agent serves as a substrate of KatG Compound I (*10*, *11*), consistent with a mechanism of drug "activation" involving a classical peroxidase cycle even though the physiological role of KatG is to serve as a catalase. KatG mutants from drug-resistant *M. tuberculosis* strains would be expected to function poorly in catalytic drug activation. The purified mutant enzyme KatG[S315T] exhibits only moderately reduced peroxidase activity when measured in vitro with typical peroxidase substrates (*11*−*13*). While this may seem to be an apparent incongruity in explaining the origin of relatively high INH resistance due to this mutation, interactions between this mutant enzyme and INH are impaired (*11*). For example, a reduced affinity of the resting (ferric) KatG[S315T] enzyme for INH was found, along with poor turnover of the drug by Compound I in this mutant (*11*). These observations alone, however, have not been extended to a description of the additional processes critical for producing bactericidal activity.

Activation or oxidation of INH alone by KatG, which was originally investigated by Johnsson et al. and others (*9*, *14*, *15*), has more recently come to be measured as production of an IN-NAD adduct molecule (Scheme 1), which is a very tight binding inhibitor of InhA (*16*−*18*). InhA, the *M. tuberculosis* enoyl-acyl carrier protein reductase, is a key enzyme involved in the biosynthesis of mycolic acids, which are components of the mycobacterial cell wall (*19*−*21*).

[†] This work was supported by National Institutes of Health Grants AI-43582 and AI-060014 (National Institute of Allergy and Infectious Diseases) and PSC-CUNY Grant 66404-0035 to R.S.M. and by the Robert A. Welch Foundation to J.C.S.

[‡] The coordinates have been deposited in the Protein Data Bank with accession codes 2CCA for WT KatG and 2CCD for the KatG[S315T] mutant.

* To whom correspondence should be addressed at Brooklyn College. Tel: 718-951-5000 ext 2845. Fax: 718-951-4607. E-mail: rmaglioz@brooklyn.cuny.edu.

[§] Brooklyn College.

[||] The Graduate Center of the City University of New York.

[⊥] Texas A&M University.

[1] Abbreviations: KatG, catalase−peroxidase; KatG[S315T], S315T mutant of KatG; HRP, horseradish peroxidase; EPR, electron paramagnetic resonance; BLC, bovine liver catalase; INH, isonicotinic acid hydrazide; DTPA, diethylenetriaminepentaacetic acid; G/GOx, glucose/glucose oxidase; SOD, superoxide dismutase; MIC, minimum inhibitory concentration.

10.1021/bi051967o CCC: $33.50
Published on Web 03/10/2006

Scheme 1: IN-NAD Adduct[a]

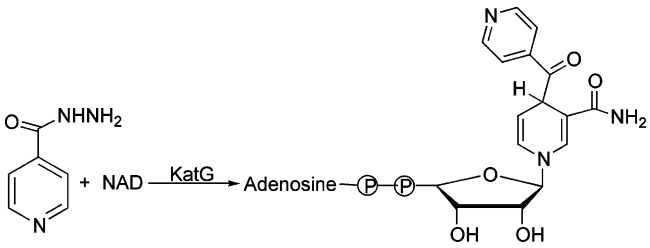

[a] The structure of the adduct is adapted from ref *17*.

Inactivation of InhA alone is sufficient to inhibit mycolic acid biosynthesis and induce cell lysis very rapidly after exposure of bacteria to INH (*22*).

It should be noted that KatG has been ascribed, in addition to catalase and nonspecific peroxidase activity, a manganese peroxidase activity, oxidase activity, INH-hydrazinolysis activity, and an isonicotinoyl-NAD synthase activity (*23*, *24*), leading to a complicated picture for its role in INH activation. Several reports on the IN-NAD adduct based on various synthetic approaches have focused on adduct structure and its interactions with InhA, rather than on the specific catalytic function of KatG in its formation. Additional background information relevant here includes demonstrations of the production of radicals from INH in reactions with KatG (*5*, *25*−*27*) and structural information concerning IN-NAD adducts generated under a variety of conditions (*28*−*30*).

The basic hypothesis that typical peroxidatic activity of *M. tuberculosis* KatG is sufficient for the activation of INH and is also applicable to explain drug resistance in KatG-[S315T] mutants has never been directly demonstrated in vitro. Experimental approaches that include oxidants or prooxidants, such as free manganese or superoxide (*24*, *31*, *32*), have been investigated to overcome an assumed lack of catalytic competence of KatG in the presence of hydrogen peroxide. A widely published superoxide-mediated mechanism for INH activation by KatG in vitro, presented by other groups (*31*−*33*), raises issues of physiological relevance since *M. tuberculosis* expresses and secretes SOD enzymes colocalized with KatG (*32*). Manganese has been frequently used as an enzyme surrogate or has been added to IN-NAD adduct-forming reactions with KatG apparently to increase yields but without explanation for its mechanistic role (*29*). Even though this approach can provide significant quantities of adduct, it is questionable that free manganese is important in antimycobacterial function under physiological conditions.

Hydrogen peroxide (H_2O_2) is an abundant oxidant in aerobic bacteria (*34*) especially relevant for intracellular pathogens such as *M. tuberculosis*. Genetic studies showed that KatG is the key enzyme responsible for mycobacterial survival during attack by reactive oxygen intermediates from the host (*35*) as it is the only catalase in this pathogen. The role of H_2O_2 in the activation of INH by *M. tuberculosis* KatG has not been carefully examined because of the underlying problem of dual activities strongly dominated by catalase activity. More critically important to the present work are reports in which alteration in a peroxidase-based activation of INH by KatG has been specifically rejected as an origin for drug resistance in the KatG[S315T] mutant enzyme (*31*, *33*).

In this report, we have chosen to adopt a physiologically relevant approach to characterize the competence of KatG and KatG[S315T] in producing InhA inhibition due to formation of the IN-NAD adduct (InhA inhibitor) to provide clues about the mechanism. Here, we demonstrate that KatG can efficiently catalyze IN-NAD adduct formation in the presence of very dilute H_2O_2 and show the poor catalytic function of the S315T mutant under similar conditions. These results sharply contrast with several other reports in which this mutant did not behave differently from wild-type enzyme under conditions designed to compare peroxidase activity in the process of adduct formation or INH oxidation (*31*, *33*).

We also pursued the solution of the three-dimensional X-ray crystal structure of the KatG[S315T] variant from *M. tuberculosis* with the aim of gaining a more complete understanding of drug activation and the resistance mechanism. The crystal structure of *M. tuberculosis* wild-type KatG has been reported (*36*). However, the structure of the *M. tuberculosis* KatG[S315T] mutant was not available and is presented here. Insights into the mechanism of INH activation emerge from our work.

EXPERIMENTAL PROCEDURES

Glucose (enzyme grade) was purchased from Fisher Scientific; 2× crystallized bovine liver catalase, glucose oxidase (from *Aspergillus niger*, low in catalase), NADH, INH, *o*-dianisidine, and all the other chemicals were bought from Sigma-Aldrich and were of the highest purity available. 2-*trans*-Dodecenoyl-CoA is a gift from Jacobus Pharmaceutical Co. INH was recrystallized from methanol and stored at 4 °C. All solutions of INH, β-NADH, and β-NAD^+ were each freshly prepared for all experiments due to the relatively rapid decomposition of INH or NADH in aqueous solution or buffer.

The *M. tuberculosis* InhA was expressed and purified as previously described (*21*).

M. tuberculosis KatG and its S315T mutant were constructed, expressed, and purified as previously described (*10*, *11*, *37*). Active KatG concentration was expressed as heme concentration ($\epsilon_{407nm} = 100\ mM^{-1}\ cm^{-1}$).

Inactivation of InhA by Isoniazid. InhA (1.0 μM) was incubated with 0.5 μM KatG or KatG[S315T] mutant, 50 μM NAD^+ (or NADH in some experiments), 50 μM isoniazid, and 2 mM EDTA in a total volume of 1.0 mL at 25 °C in 20 mM phosphate buffer, pH 7.2. Glycerol (8% v/v) and bovine serum albumin (0.1 mg/mL) were also included to stabilize InhA (*9*). Aliquots (30 μL) were taken at defined time points, and residual InhA activity was measured following the loss of absorbance of NADH at 340 nm using 2-*trans*-dodecenoyl-CoA (100 μM) and excess NADH (200 μM) as substrates for this assay. Specific activity was calculated as micromoles of NADH ($\epsilon_{340} = 6220\ M^{-1}\ cm^{-1}$) oxidized per minute per milligram of InhA. The InhA residual activities at various time points were expressed relative to 100%, which is the value measured at time zero.

Enzymatic Generation of H_2O_2. H_2O_2 was generated using glucose/glucose oxidase (G/GOx): GOx (10 mU), together with 5 mM glucose, was added to the activation mixture described above. The rate of hydrogen peroxide release by the G/GOx system was determined separately using an HRP-coupled *o*-dianisidine oxidation assay. Oxygen concentration in air-saturated solutions is approximately 0.2 mM, a large

excess relative to the rate of turnover of the oxidase. In the presence of 10 milliunits/mL GOx, the rate of H_2O_2 production was shown to be 2.0 μM/min.

Effects of Catalase and o-Dianisidine. Bovine liver catalase (0.5 μM, heme concentration) or *o*-dianisidine (200 μM) was added directly to reaction mixtures containing KatG, INH, NADH, and InhA as described above. The InhA residual activity was measured accordingly in aliquots removed at defined time points as above.

Trapping of the IN-NAD Adduct by InhA. The inhibitor generated in reaction mixtures containing INH, NAD^+, KatG, and G/GOx in the absence of InhA was isolated according to Lei et al. (*18*) with minor modification. Briefly, 1 mL of 20 mM phosphate buffer (pH 7.2) containing KatG (1 μM), INH (200 μM), NAD^+ (200 μM), GOx (40 mU), and glucose (5 mM) was incubated aerobically at room temperature for 50 min. The reaction was terminated by the removal of KatG and GOx through ultrafiltration. The filtrate was mixed with InhA and incubated at room temperature for 20 min to ensure equilibration of InhA with inhibitor. The InhA−inhibitor complex was isolated through gel filtration, and its optical spectrum showed a shoulder at 320 nm that is absent from the spectrum of pure InhA. This absorbance is due to the tightly bound IN-NAD adduct and reproduces results reported elsewhere (*18*). When GOx was omitted, the absorbance at 320 nm was not detectable in the recovered InhA. The free IN-NAD adduct was isolated from the InhA−adduct complex to confirm its identity. Its spectrum showed characteristic absorbance peaks at 260 and 326 nm, in agreement with previously reported data (*16*, *18*, 26).

INH Concentration Dependence of IN-NAD Formation. The rates of IN-NAD adduct generation with varying concentrations of INH were examined directly with either KatG or the KatG[S315T] mutant in a spectrophotometric assay. This study was carried out in the absence of InhA, using KatG (0.5 μM), NAD^+ (50 μM), GOx (10 milliunuts/mL), and glucose (5 mM). Free NAD^+ shows no absorbance at 326 nm, which is a characteristic absorbance peak of the IN-NAD molecule. The generation of adduct was initiated by the addition of varying amounts of INH (5, 10, 20, 30, and 50 μM). In the case of the KatG[S315T] mutant, higher concentrations of INH (0.25, 0.5, 1, and 2 mM) were required to achieve detectable increases in absorbance in reasonable time periods. To monitor adduct formation, the absorbance at 326 nm was recorded for 20 min after the addition of INH. The concentration of the IN-NAD adduct was calculated according to its extinction coefficient ($\epsilon_{326nm} = 6900$ M^{-1} cm^{-1}) (*16*, *18*), an approach similar to that described by Singh et al. (*24*). The reference cuvette contained all components except NAD^+ to correct for background. The initial rate of adduct formation was computed from the absorbance change during the first 5 min.

Crystallization, Data Collection, and Structure Determination/Refinement. Crystals of native KatG and the mutant KatG[S315T] were grown by sitting-drop vapor diffusion in well solutions containing 100 mM sodium acetate, pH 4.6, 6% PEG 4000, and 0.17 mM *n*-dodecyl β-D-maltoside at 24−27 mg/mL protein concentrations. Crystals were cryoprotected in 25% glycerol mixed with well solution and were then flash-frozen in liquid nitrogen. Data were collected using synchrotron radiation either at the Advanced Light Source, Berkeley, CA (for KatG[S315]), or at the ID-C beamline of the Advanced Photon Source at Argonne National Laboratory, Chicago, IL. Data were collected at 100 K to a resolution of 2.1 Å (KatG[S315]) or 2.0 Å (WT KatG). The data were processed with HKL2000 (*38*). Crystals of both enzymes belong to space group $P4_22_12$ with cell dimensions $a = b = 150$ Å, $c = 154$ Å, $\alpha = \beta = \gamma = 90°$. The crystal structure of WT KatG was solved by molecular replacement using the program MolRep (*39*) with *Burkholderia pseudomallei* KatG (1MWV) as the search model. The resulting model was initially refined to 2.7 Å resolution with strict noncrystallographic restraints using REFMAC5 (*40*) followed by model building using TEXTAL (*41*). The model was refined by simulated annealing as implemented in CNS (*42*) and further built and refined in Xtalview (*43*). The phases were improved and extended to 2.0 Å resolution with Shake&wARP (*44*), and the model was refined using REFMAC5. The crystal structure of KatG[S315T] was refined using WT KatG as a model. The quality of the structures was validated using PROCHECK (*45*).

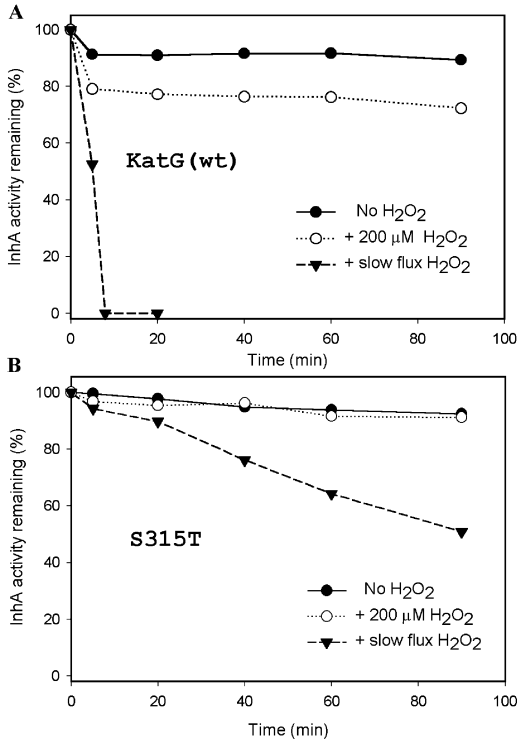

FIGURE 1: Inhibition of InhA activity by INH catalyzed by KatG or its [S315T] mutant. InhA (1 μM) was incubated with 2 mM EDTA, INH (50 μM), NAD^+ (50 μM), and KatG (0.5 μM) at 25 °C: (●) no H_2O_2 added; (○) 200 μM H_2O_2 added at time zero; (▼) with continuous flux of H_2O_2 (2 μM/min, generated enzymatically). Panels: (A) mediated by KatG; (B) mediated by the KatG-[S315T] mutant. Data points are the means of three independent results with SE less than 5%.

RESULTS

Inactivation of InhA by INH Catalyzed by KatG. The first goal of this work is to identify a mechanism whereby KatG mediates InhA inhibition in the absence of exogenous peroxide. As shown in Figure 1A, there was low level inhibition of InhA activity (~8%) only at the earliest time point during incubation of a mixture of INH, ferric KatG, and NAD^+. As becomes clear below, the initial yield of inhibitor is likely due to small amounts of hydrogen peroxide

present in the solution, most of which is likely due to autoxidation of INH (*46*), which initiated the KatG peroxidase cycle. In the absence of KatG, the inhibition of InhA activity was negligible (data not shown).

To then directly test the effect of hydrogen peroxide, 200 μM H_2O_2 was added to the reaction mixture. Enhanced inhibition (~20%) of InhA was observed but only within the first 5 min. A constant flux (2 μM/min) of H_2O_2 from an enzymatic source in the presence of 50 μM INH and NAD^+ was found to drive complete inhibition of 1.0 μM InhA in only 8 min (Figure 1A).

In a control experiment, when INH was omitted, InhA maintained its full activity over 1.5 h of incubation under the same conditions (2 μM/min H_2O_2) (data not shown). H_2O_2 alone can cause a low level of InhA inactivation, for example, a 10-fold excess of authentic H_2O_2 inhibited InhA activity by 12% over 1 h. This background inhibition was not seen in the above-described control experiment, in which KatG was present. Thus, the observed rapid inhibition of InhA was not the consequence of a direct attack of H_2O_2 on InhA.

As described in the Experimental Procedures section, a significant amount of the IN-NAD adduct was trapped, purified, and optically characterized from the mixture of KatG-mediated INH activation (with slow flux H_2O_2). These results suggest that inhibition of InhA observed here occurs through the production of the IN-NAD adduct that binds tightly to the active site of InhA. Since the concentration of H_2O_2 was very low here, KatG Compound I would be expected to be the reactive enzyme intermediate present at a steady-state level low enough to minimize catalase activity.

An enhancement of InhA inhibition was also achieved (data not shown) using an automatic titration apparatus by multiple injections of limiting amounts of H_2O_2 (approximately 0.5 equiv per heme per injection over a period of 1 h) into the INH, NAD^+, and InhA reaction mixture with KatG.

Having found an approach that could provide mechanistic insights, we proceeded to probe the function of the drug-resistant mutant KatG[S315T]. As above, adding one aliquot of 200 μM H_2O_2 yielded minimal inactivation of InhA (Figure 1B). When a constant flux of H_2O_2 was included, 50% inhibition was found after 90 min (Figure 1B). The rate of inhibition of InhA mediated by the mutant is 5% of that produced by wild-type KatG and was not enhanced when the flux of peroxide was doubled. This is different from the behavior of the wild-type enzyme for which the rate increases when increasing the peroxide flux.

Comparison of NAD^+ and NADH. In the absence of added peroxide, significant inhibition of InhA occurs in the mixture of INH, NADH, and KatG (Figure 2A). As shown above, the extent of inhibition was minimal when NAD^+ is used under these conditions, yet NAD^+ is clearly a reactant in the presence of peroxide as shown above. Since NADH can give rise to small amounts of superoxide and H_2O_2, nonenzymatically (*47*) and/or through the reported KatG oxidase activity (*24*), and NAD^+ would not, the effect of scavenging H_2O_2 was tested. As shown in Figure 2A, in the presence of 0.5 μM bovine liver catalase (BLC, heme concentration), the inhibition of InhA was greatly reduced. The residual inhibition probably reflects the likelihood that the added BLC does not out-compete KatG for the H_2O_2 present in the mixture and initiation of catalysis by Compound I in KatG still persists. Both KatG and BLC have similar k_{cat}/K_m values for catalase turnover (*48*, *49*). Another possibility is that trace amounts of superoxide could initiate adduct formation.

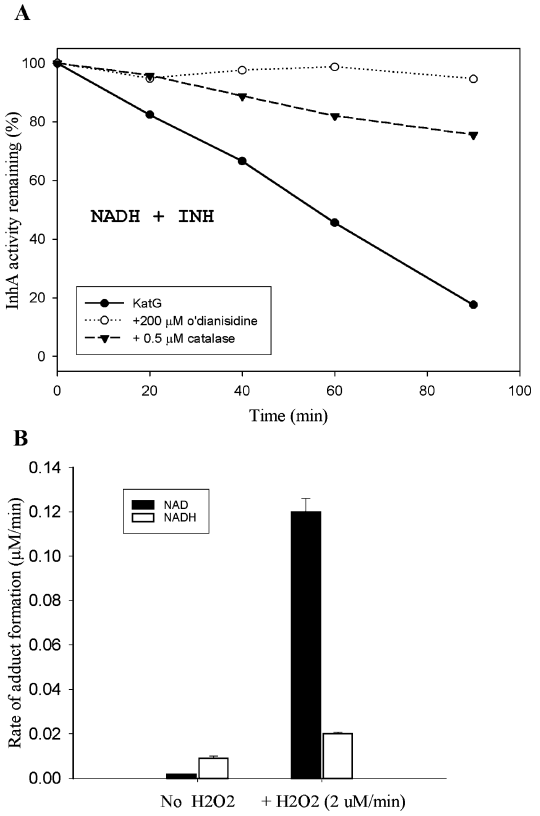

FIGURE 2: Inhibition of InhA activity by INH and NADH catalyzed by KatG. (A) InhA (1 μM) was incubated with INH (50 μM), NADH (50 μM), and KatG (0.5 μM) at 25 °C. (B) Adduct formation rates were compared using NADH vs NAD^+. Rates were calculated on the basis of the loss of InhA activity over 40 min of incubation under conditions described in Figure 1, assuming that InhA was inhibited by a stoichiometric binding of adduct. H_2O_2 was generated enzymatically. Results are the means and ranges of duplicate determinations.

To further explore the mechanism of these reactions without added peroxide, *o*-dianisidine, a peroxidase substrate, was tested for its ability to interfere with inhibitor production. In the presence of 200 μM *o*-dianisidine, the rate of inhibition of InhA was greatly reduced, suggesting that the production of the IN-NAD adduct was effectively blocked by competition for KatG peroxidase intermediates by *o*-dianisidine (Figure 2A) (tested in the presence of NADH).

Both NAD^+ and NADH have been used in other in vitro approaches focused on INH activation. Recently, there is an increasing awareness that NAD^+ might be the "trap" for an isonicotinoyl radical produced from INH (*24*, *28*), and therefore, NADH cannot be a cosubstrate. Here, in the absence of added H_2O_2, NADH was much *more* efficient than NAD^+ in producing inhibition of InhA (Figure 2B). When sufficient exogenous H_2O_2 (2 μM/min) was included, NAD^+ provided a 5-fold greater efficiency in adduct formation (Figure 2B) compared to equivalent amounts of NADH. This apparent contradiction has never been addressed before and is consistent with NADH oxidation supplying H_2O_2 for initiation of the KatG peroxidation pathway that is not present when NAD^+ is used. These results suggest that the stimulating effect of NADH relative to NAD^+ in the absence of added peroxide is partially compromised by its role as a

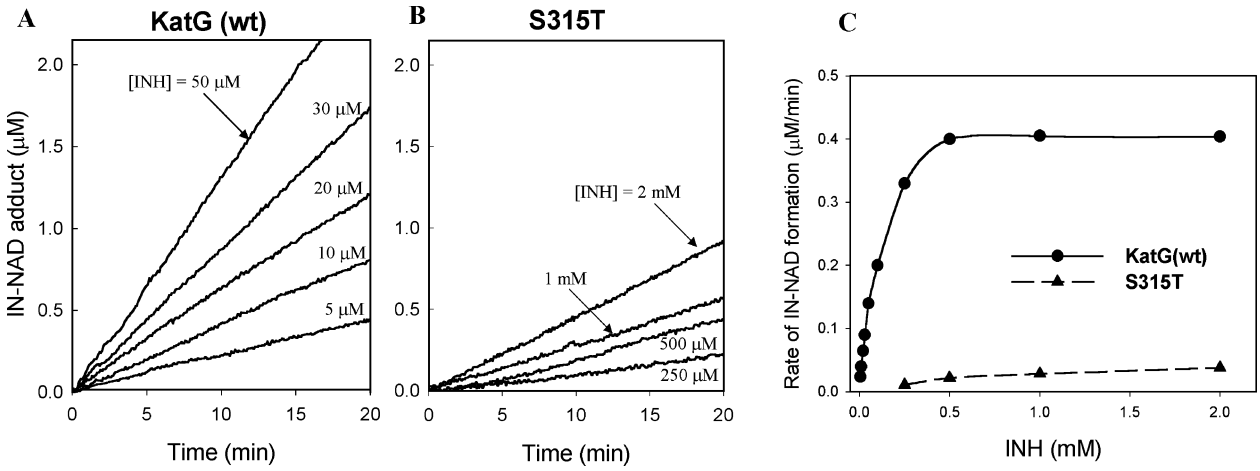

FIGURE 3: Effect of INH concentration on the production of the IN-NAD adduct. IN-NAD adduct formation was monitored by its characteristic absorbance at 326 nm. KatG (0.5 μM), NAD^+ (50 μM), and H_2O_2 (2 μM/min, generated enzymatically) were incubated with varying amounts of INH. (A) wild-type KatG and 5, 10, 20, 30, and 50 mM INH; (B) S315T mutant and 0.25, 0.5, 1, and 2 mM INH. (C) Initial rates (first 5 min) of adduct formation as a function of INH concentration calculated on the basis of experiments as described in (A) and (B).

reducing substrate for KatG Compound I when exogenous H_2O_2 was supplied.

INH and NAD^+ Concentration Dependence. Free IN-NAD adduct has a characteristic absorbance at 326 nm, a wavelength at which NAD^+, INH, and its oxidation products show no significant absorbance. Therefore, the generation of IN-NAD can be monitored spectrophotometrically in reaction mixtures containing KatG, drug, and dinucleotide cofactor in the absence of InhA. When any of the three components was omitted, there was no detectable absorbance increase at 326 nm (in the presence of G/GOx). As shown in Figure 3A, when the amount of NAD^+ is fixed at 50 μM, the yield of the IN-NAD adduct was dependent on INH concentration. These results demonstrate for the first time that KatG activation of the drug is consistent with a reaction mechanism that depends on the rate-limiting oxidation of INH. The present results are also in good quantitative agreement with the InhA inhibition approach described above. For example, using 50 μM INH, 1.0 μM inhibitor was produced in 7.6 min, in agreement with complete inhibition of 1 μM InhA in 8 min as shown in Figure 1A. Interestingly, the KatG-[S315T] mutant required concentrations of INH hundreds-fold higher than those used with wild-type KatG to produce the IN-NAD adduct at appreciable rates (Figure 3B).

The hydrogen peroxide supplied was fixed at 2 μM/min in this set of experiments, and INH concentration was increased to establish a V_{max} for the IN-NAD generation process. Under these conditions, a maximum rate of 0.4 μM adduct/min was reached using 500 μM INH (Figure 3C). No attempt was made to achieve a maximum rate for the mutant enzyme because of the very high concentrations of INH that would have been required. Separate experiments showed that, for wild-type KatG, lower peroxide flux produced less inhibitor as expected for a mechanism dependent on the steady-state concentration of Compound I (data not shown) at constant INH concentration. The behavior shown in Figure 3 demonstrates for the first time that the rate of adduct formation obeys saturation kinetics and thus a specific interaction between KatG and the drug.

In the presence of 50 μM INH, adduct yield did not change when the concentration of NAD^+ was varied from 25 to 200 μM. This result provides strong evidence that the rate-limiting reaction in adduct formation is the peroxidation of INH alone, that NAD^+ is efficient at scavenging an INH-derived intermediate, and that it does not compete for Compound I in the concentration range used here. Furthermore, dinucleotide radicals, which are potentially produced through peroxidation of NADH, are not necessary for adduct formation.

IN-NAD Adduct Formation Using tert-Butyl Hydroperoxide. *tert*-Butyl hydroperoxide (*t*-ButOOH) has been used in other reports leading to the conclusion that the peroxidatic cycle of KatG *is not* responsible for drug activation, since WT and S315T mutant enzymes showed little difference in behavior (*31*, *32*). With NAD^+ as cosubstrate, adduct production was carefully monitored here using *t*-ButOOH. In the first 2 min, WT KatG was about 10 times more efficient than the mutant in producing InhA inhibitor, while the total amount of adduct produced in 10 min by WT KatG was more than 6-fold that produced by the S315T mutant. Unlike the H_2O_2-mediated reaction system, the rate of adduct formation declined with incubation time for both WT and S315T in the presence of *t*-ButOOH but was more obvious with the WT enzyme (Figure 4). It is likely that the high concentration of this alkyl peroxide leads to enzyme inhibition or degradation during turnover. Therefore, prior studies, in which INH oxidation or adduct formation was measured after long incubation times (*31*, *32*), could not provide an accurate comparison of catalytic efficiency in the WT and mutant enzymes.

Three-Dimensional Crystal Structure of the KatG[S315T] Mutant. The overall structure of the *M. tuberculosis* KatG-[S315T] mutant (PDB code 2CCD), including the arrangement of catalytically important residues surrounding the heme, is the same as the wild-type enzyme (also solved here, PDB code 2CCA). Crystallographic *R* factor (23%) and R_{free} (28%) and other refinement statistics are similar to those in wild-type KatG (*R* and R_{free} factors of 20% and 23%) (Table 1). This observation is consistent with the relatively unaltered catalase and peroxidase activities of the purified mutant enzyme.

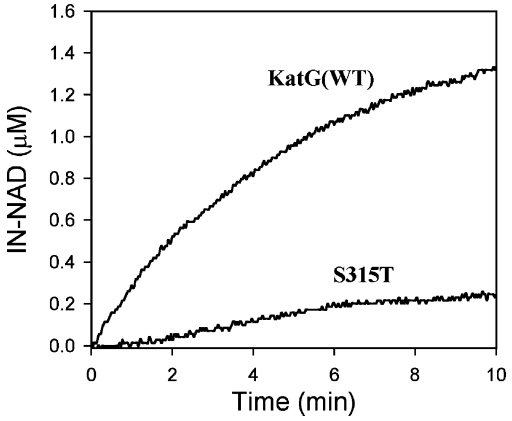

FIGURE 4: KatG- and S315T-mediated IN-NAD adduct formation using *tert*-butyl hydroperoxide. WT KatG or S315T mutant (1 μM), INH (200 μM), NAD^+ (100 μM), and *tert*-ButOOH (400 μM) were incubated at room temperature for 10 min. DTPA (0.1 mM) was included to minimize the effects of metal ions. IN-NAD adduct formation was monitored by its characteristic absorbance at 326 nm. Measurements were repeated twice, and similar results were observed.

Table 1: Data Collection and Structure Refinement Statistics for *M. tuberculosis* KatG and the KatG[S315T] Mutant

	KatG (WT)	KatG[S315T]
(A) data collection statistics		
wavelength (Å)	0.90	0.97
unit cell parameters		
a (Å)	150.1	149.8
b (Å)	150.1	149.8
c (Å)	153.7	154.5
space group	$P4_22_12$	$P4_22_12$
resolution limits (Å)	2.0	2.1
unique reflections	105049	76312
completeness (%)	99.0 (96.7)	78.5 (64.0)[a]
R_{sym}[b] (%)	8.3 (35.1)	11.8 (28.3)
I/σ	26.2 (4.5)	9.4 (2.1)
(B) refinement statistics		
resolution range (Å)	20.0−2.0	20.0−2.1
test set size (%)	5	5.1
R_{cryst}[c] (%)	19.8	23.0
R_{free}[d] (%)	22.9	27.6
no. of non-H protein atoms	12063	11749
no. of water molecules	938	596
rmsd of bond angles (deg)	1.26	1.39
average *B* value (Å)	23.93	20.28
Ramachandran plot		
most favored (%)	90.3	89.6
additionally allowed (%)	9.4	10.2
generously allowed (%)	0.3	0.2
disallowed (%)	0.0	0.0

[a] Numbers in parentheses represent values in the highest resolution shell. [b] $R_{sym} = \sum_h\sum_i|I(h,i) - \langle I(h)\rangle|/\sum_h\sum_i I(h,i)$, where $I(h,i)$ is the intensity value of $I(h)$ for all i measurements. [c] $R_{cryst} = \sum||F_o| - |F_c||/\sum|F_o|$, where $|F_o|$ and $|F_c|$ are the observed and calculated structure factor amplitudes, respectively. [d] R_{free} is the same as R_{cryst} but calculated with a 5% subset of all reflections that was never used in any refinement.

The distal side of the heme pocket connects to the molecular surface through a long substrate access channel that is delimited by Ser315 and the carboxyl group of Asp137 at its narrowest point close to the heme edge. The narrow neck in the channel creates a steric barrier for access to the heme active site. The most important change in the mutant structure is due to the presence of the methyl group of the Thr315 side chain. The methyl group introduced by Thr315 effectively constricts the accessibility to the heme by closing

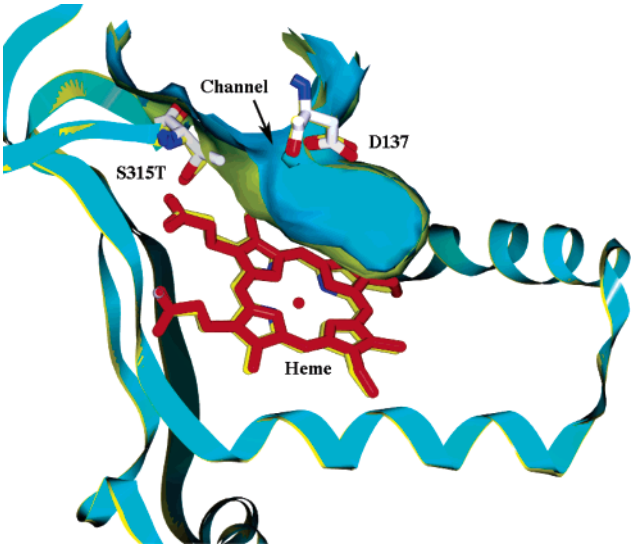

FIGURE 5: Structural comparison of *M. tuberculosis* wild-type KatG and the KatG[S315T] mutant around the substrate access channel. The figure was constructed using the graphic program SPOCK (*65*) with superimposed wild-type and mutant structures. Molecular surfaces were calculated and are displayed in yellow for wild-type KatG and in blue for the S315T mutant. The substrate access channel to the distal side of the heme is displayed within a distance of 10 Å from heme iron. Residues Asp137 and Thr315 are shown in stick representation. The carbon atoms of these residues are colored yellow for the WT KatG and white for the mutant. The heme in KatG[S315] is colored red. The heme in WT KatG is colored yellow for carbon, red for oxygen, and blue for nitrogen. The ribbon diagram of the mutant is colored in light blue and superimposed on that of wild-type KatG in yellow.

down the dimensions of the narrowest part of the channel from 6 Å in the WT KatG to 4.7 Å in the mutant (Figure 5). Another notable difference in the mutant KatG lies in the solvent organization both in the major access channel and in the distal side of the heme pocket (see figure in Supporting Information). Specifically, the structural water molecule (W261) coordinated to the heme iron (iron−oxygen distance = 2.9 Å) in WT KatG was not seen in KatG[S315T]. The water molecule hydrogen bonded to Nϵ of Arg104 is retained in both structures (W20 or W336). The absence of the iron-coordinated water in the *M. tuberculosis* mutant is consistent with spectroscopic measurements (EPR, optical, and resonance Raman) in which 5-coordinate heme iron was identified in KatG[315T], in the freshly prepared enzyme, and after storage and at low pH (*50*).

The indole nitrogen atom of Trp107 in *M. tuberculosis* KatG[S315T] is modified as reported for Trp111 in the *B. pseudomallei* KatG[S324T] mutant, but such modification was not found in WT KatG from either organism. The origins and implications of these changes were not investigated further. No confirmation of a specific INH binding site as proposed in previous studies (*50*−*54*) could be obtained in wild-type KatG crystals either through cocrystallization or through soaking in the presence of INH.

DISCUSSION

A collection of reports appeared over the past several years in which the catalytic role of KatG in INH activation was examined under conditions in which a specific role for hydrogen peroxide may have been obscured or irrelevant. The fact that WT KatG and the S315T mutant exhibit similar

Scheme 2: Proposed Mechanism of INH Activation by KatG[a]

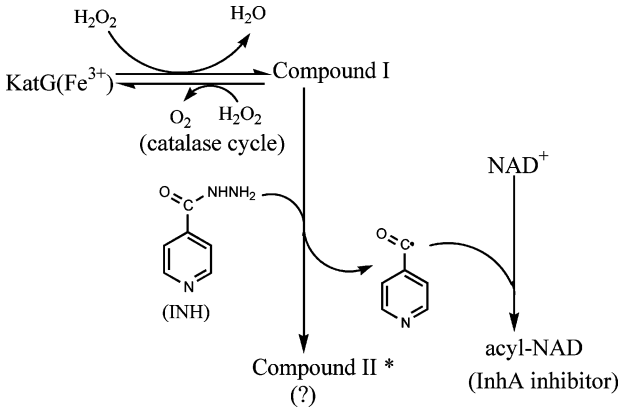

[a] The asterisk indicates not yet identified.

peroxidase activity and reports that both enzymes oxidize INH and also generate IN-NAD adduct at similar rates when using alkyl peroxide (*t*-ButOOH) (*32*) obscured a simple description of the origins of INH resistance. Furthermore, previous studies have shown that direct addition of bulk H_2O_2 to resting KatG does not lead to peroxidation of INH (*46*) nor the generation of the IN-NAD adduct (*31*). In this study, however, we directly demonstrated that both H_2O_2 and *t*-ButOOH efficiently mediate InhA inhibitor formation and also that WT KatG and the S315T mutant exhibit significant differences when these peroxides are present. We also found that the peroxide-mediated INH activation is not affected by SOD and does not require manganese. Thus, peroxidatic activity of KatG is sufficient to account for drug activation and INH resistance caused by the S315T mutation. Suggestions that this was the case were provided by recent results concerning IN-NAD adduct formation by the KatG from *B. pseudomallei* in the presence of manganese (*24*) and by the demonstration that a slow flux of hydrogen peroxide could initiate radical production in a coupled reaction using ferric KatG, INH, and NBT (*26*, *55*). Those reports, however, did not present a detailed mechanism for adduct formation in the context of peroxidase-based catalytic function of KatG.

H_2O_2 is produced in actively growing cells as a result of aerobic metabolism. In *M. tuberculosis* infection, the pathogen is also exposed to large amounts of H_2O_2 released by macrophages. As the only catalase in *M.* tuberculosis, KatG is the principal H_2O_2 scavenger protecting against oxidative stress, which was clearly demonstrated in a KatG knockout strain of *M. tuberculosis* (*35*).

Both the catalase and the peroxidase cycles in KatG share a common intermediate, Compound I. A very low level of H_2O_2 would be expected to limit the rate of catalase turnover and still support Compound I formation, which can then be diverted in the presence of an oxidizable substrate such as INH. Under such circumstances, peroxidation can occur as a "side reaction" that competes with turnover of H_2O_2. The relative rates of the two pathways would be expected to depend on affinities of competing substrates, H_2O_2 and INH, for reaction with KatG Compound I (Scheme 2), as we have shown. The peroxidase activity of mammalian catalase when H_2O_2 is at low levels may be related to this observation (*56*).

A continuous flow of dilute H_2O_2 producing very small amounts of Compound I could simulate the physiological environment in which drug activation and inhibition of InhA takes place. KatG is localized near the surface of mycobacteria (in a periplasmic-type space) and is also secreted by this pathogen, while SOD is also present in those areas (*57*, *58*). Thus, in the presence of INH, all components, including H_2O_2, needed to generate the InhA inhibitor, are likely to be localized together. This issue has not received any attention in the recent literature. The difference in rates of adduct formation between WT KatG and KatG[S315T] found here is consistent with reports that *M. tuberculosis* strains bearing the S315T mutation are still susceptible to INH but with MICs up to 180-fold (0.5 vs 90 μg/mL) higher than that for wild-type strains (*59*−*61*). In this regard, H_2O_2-mediated KatG activation of INH models a physiologically relevant route.

A clear demonstration of the conditions that explain the susceptibility in vitro of INH-resistant strains bearing KatG-[S315T] emerges here. Earlier in vitro experiments on INH resistance in KatG[S315T] used very large excesses of alkyl peroxide added to the ferric enzyme, or superoxide plus the ferric enzyme, or even an unusual peroxide (MPPH) reported to provide a direct route to Compound II from the ferric enzyme, to test for a mechanism-based origin of INH resistance. These reports showed either no function of the mutant or the same function of the mutant and wild-type enzyme, depending on the chosen conditions (*31*−*33*). None of these reports shed light on a drug activation mechanism that accommodates susceptibility of mutant strains in vitro but resistance under normal therapeutic dosing.

If H_2O_2 is taken as the most likely oxidant molecule encountered by ferric KatG in vivo, it is likely that the rate-limiting step for InhA inhibitor formation, given a constant ratio of NAD^+/NADH, is peroxidation of INH leading to a reactive acylating radical or anion. The generation of radical intermediates from INH by KatG has been directly shown (*62*), while attack of this or other intermediates on the nicotinamide ring of NAD^+ to form the IN-NAD adduct/InhA inhibitor still needs to be directly demonstrated. In this study, the results using NAD^+ rather than NADH also provided greater insights into the mechanism of IN-NAD adduct formation. A reasonable explanation for the lack of requirement for exogenous peroxide to generate the adduct in the presence of NADH derives from the autoxidation of NADH (and also INH) in aerobic solution and the idea that, at neutral pH, reactive oxygen species (H_2O_2 and superoxide) produced by such a route can initiate catalysis by KatG. Unlike the *B. pseudomallei* KatG, *M. tuberculosis* KatG exhibits very low NADH oxidase activity (*24*), and therefore, autoxidation of NADH (or INH) alone provides an adequate source of peroxide under the conditions used here.

Other studies showed that KatG-mediated IN-NAD adduct formation can be accelerated by including manganese or superoxide. Manganese, whether introduced in the +2 or +3 state, is redox active such that Mn^{3+} is able to rapidly oxidize INH (*23*) and Mn^{2+} can generate superoxide (*9*, *32*) in aerobic systems. Adduct formation in the presence of manganese might therefore be analogous to the use of exogenous superoxide (*31*, *33*) in addition to directly producing radicals from INH. Superoxide-related INH activation would be less physiologically interesting however, compared to peroxidase catalysis, if these are in fact independent, since SOD enzymes coexist with KatG in vivo.

Interestingly, SOD has been shown to block metal ion mediated INH oxidation by KatG (*32*).

KatG Compound III (oxyferrous KatG) had been concluded to be an obligatory intermediate in INH activation, while in KatG[S315T], this intermediate was assigned as being nonfunctional (*31*) in explanation of the origin of INH resistance. Whether a direct or indirect route to KatG Compound III exists in vivo has not been addressed by other authors. A more recent report suggests that Compound II of catalase−peroxidase, defined as an intermediate containing ferric heme iron and a protein-based radical, may also be important in explaining drug resistance (*63*). Little is known about how a protein-based radical in the KatG Compound II intermediate catalyzes INH activation by KatG or how this intermediate (or its lack) in the S315T mutant enzyme could be responsible for INH resistance.

The WT KatG structure solved here shows heme iron to be 6-coordinate, different from the previously solved structure in which heme iron is 5-coordinate (*36*). This observation confirms our report that 6-coordinate heme iron with a water bound becomes more abundant during storage of the enzyme after purification and at low pH (*64*). The mutation of Ser315 or Ser324 (*B. pseudomallei* KatG) to Thr narrows the heme access channel from around 6 to 4.7 Å at its narrowest point in the mutant enzymes from both organisms. These observations and the significantly decreased INH activation function in these mutants (*52*) suggest that drug binding within the heme pocket is a likely requirement for INH activation.

Our results help to explain the origin of INH resistance in strains bearing the S315T mutation in *M. tuberculosis* KatG. In this mutant, the yield of inhibitor only becomes significant when high concentrations of INH are available, under conditions that we propose allow other aspects of the generation of the inhibitor process to occur in nonenzymatic reactions. This is completely consistent with the features of the mutant structure reported here in that the replacement of threonine for serine produces steric effects that interfere with interaction between the enzyme and INH but do not interfere with formation of Compound I from small peroxide molecules such as H_2O_2 (*11*).

In conclusion, the data presented here demonstrate a simple but physiologically relevant scheme that explains the mechanism for the rapid bactericidal effects of INH resulting from the role of KatG in INH activation consistent with well-characterized structural and functional properties of the wild-type and drug-resistant enzymes.

ACKNOWLEDGMENT

Thanks to Li-Wei Hung and Minmin Yu for the data collection on the KatG[S315T] mutant. Use of the Advanced Photon Source was supported by the U.S. Department of Energy, Office of Science, Office of Basic Energy Sciences, under Contract W-31-109-Eng-38.

SUPPORTING INFORMATION AVAILABLE

One figure showing the arrangement of water molecules in the active site of both enzymes. This material is available free of charge via the Internet at http://pubs.acs.org.

REFERENCES

1. Middlebrook, G., Cohn, M. L., and Schaeffer, W. B. (1954) *Am. Rev. Tuberc. 70*, 852−872.
2. Robitzek, E. H., and Selikoff, I. J. (1952) *Am. Rev. Tuberc. 65*, 402−410.
3. Zhang, Y., Garbe, T., and Young, D. (1993) Transformation with katG restores isoniazid-sensitivity in *Mycobacterium tuberculosis* isolates resistant to a range of drug concentrations, *Mol. Microbiol. 8*, 521−524.
4. Zhang, Y., Heym, B., Allen, B., Young, D., and Cole, S. (1992) The catalase-peroxidase gene and isoniazid resistance of *Mycobacterium tuberculosis*, *Nature 358*, 591−593.
5. Rouse, D. A., DeVito, J. A., Li, Z., Byer, H., and Morris, S. L. (1996) Site-directed mutagenesis of the katG gene of *Mycobacterium tuberculosis*: effects on catalase-peroxidase activities and isoniazid resistance, *Mol. Microbiol. 22*, 583−592.
6. Musser, J. M. (1996) Molecular population genetic analysis of emerged bacterial pathogens: selected insights, *Emerging Infect. Dis. 2*, 1−17.
7. Marttila, H. J., Soini, H., Eerola, E., Vyshnevskaya, E., Vyshnevskiy, B. I., Otten, T. F., Vasilyef, A. V., and Viljanen, M. K. (1998) A Ser315Thr substitution in KatG is predominant in genetically heterogeneous multidrug-resistant *Mycobacterium tuberculosis* isolates originating from the St. Petersburg area in Russia, *Antimicrob. Agents Chemother. 42*, 2443−2445.
8. Marttila, H. J., Soini, H., Huovinen, P., and Viljanen, M. K. (1996) katG mutations in isoniazid-resistant *Mycobacterium tuberculosis* isolates recovered from Finnish patients, *Antimicrob. Agents Chemother. 40*, 2187−2189.
9. Johnsson, K., King, D. S., and Schultz, P. G. (1995) Studies on the mechanism of action of isoniazid and ethionamide in the chemotherapy of tuberculosis, *J. Am. Chem. Soc. 117*, 5009−5010.
10. Chouchane, S., Lippai, I., and Magliozzo, R. S. (2000) Catalase-peroxidase (*Mycobacterium tuberculosis* KatG) catalysis and isoniazid activation, *Biochemistry 39*, 9975−9983.
11. Yu, S., Girotto, S., Lee, C., and Magliozzo, R. S. (2003) Reduced affinity for isoniazid in the S315T mutant of *Mycobacterium tuberculosis* KatG is a key factor in antibiotic resistance, *J. Biol. Chem. 278*, 14769−14775.
12. Wengenack, N. L., Uhl, J. R., St. Amand, A. L., Tomlinson, A. J., Benson, L. M., Naylor, S., Kline, B. C., Cockerill, F. R., III, and Rusnak, F. (1997) Recombinant *Mycobacterium tuberculosis* KatG(S315T) is a competent catalase-peroxidase with reduced activity toward isoniazid, *J. Infect. Dis. 176*, 722−727.
13. Saint-Joanis, B., Souchon, H., Wilming, M., Johnsson, K., Alzari, P. M., and Cole, S. T. (1999) Use of site-directed mutagenesis to probe the structure, function and isoniazid activation of the catalase/peroxidase, KatG, from *Mycobacterium tuberculosis*, *Biochem. J. 338*, 753−760.
14. Zabinski, R. F., and Blanchard, J. S. (1997) The requirement for manganese and oxygen in the isoniazid-dependent inactivation of *Mycobacterium tuberculosis* enoyl reductase, *J. Am. Chem. Soc. 119*, 2331−2332.
15. Quemard, A., Dessen, A., Sugantino, M., Jacobs, W. R. J., Sacchettini, J. C., and Blanchard, J. S. (1996) Binding of catalase-peroxidase-activated isoniazid to wild-type and mutant *Mycobacterium tuberculosis* enoyl-ACP reductases, *J. Am. Chem. Soc. 118*, 1561−1562.
16. Rawat, R., Whitty, A., and Tonge, P. J. (2003) The isoniazid-NAD adduct is a slow, tight-binding inhibitor of InhA, the *Mycobacterium tuberculosis* enoyl reductase: adduct affinity and drug resistance, *Proc. Natl. Acad. Sci. U.S.A. 100*, 13881−13886.
17. Rozwarski, D. A., Grant, G. A., Barton, D. H. R., Jacobs, W. R., Jr., and Sacchettini, J. C. (1998) Modification of the NADH of the isoniazid target (InhA) from *Mycobacterium tuberculosis*, *Science 279*, 98−102.
18. Lei, B., Wei, C. J., and Tu, S. C. (2000) Action mechanism of antitubercular isoniazid. Activation by *Mycobacterium tuberculosis* KatG, isolation, and characterization of inha inhibitor, *J. Biol. Chem. 275*, 2520−2526.
19. Banerjee, A., Dubnau, E., Quemard, A., Balasubramanian, V., Um, K. S., Wilson, T., Collins, D., de Lisle, G., and Jacobs, W. R., Jr. (1994) inhA, a gene encoding a target for isoniazid and ethionamide in *Mycobacterium tuberculosis*, *Science 263*, 227−230.
20. Dessen, A., Quemard, A., Blanchard, J. S., Jacobs, W. R., Jr., and Sacchettini, J. C. (1995) Crystal structure and function of the isoniazid target of *Mycobacterium tuberculosis*, *Science 267*, 1638−1641.
21. Quemard, A., Sacchettini, J. C., Dessen, A., Vilcheze, C., Bittman, R., Jacobs, W. R., Jr., and Blanchard, J. S. (1995) Enzymatic

characterization of the target for isoniazid in *Mycobacterium tuberculosis*, *Biochemistry 34*, 8235−8241.
22. Vilcheze, C., Morbidoni, H. R., Weisbrod, T. R., Iwamoto, H., Kuo, M., Sacchettini, J. C., and Jacobs, W. R., Jr. (2000) Inactivation of the inhA-encoded fatty acid synthase II (FASII) enoyl-acyl carrier protein reductase induces accumulation of the FASI end products and cell lysis of *Mycobacterium smegmatis*, *J. Bacteriol. 182*, 4059−4067.
23. Magliozzo, R. S., and Marcinkeviciene, J. A. (1997) The role of Mn(II)-peroxidase activity of mycobacterial catalase-peroxidase in activation of the antibiotic isoniazid, *J. Biol. Chem. 272*, 8867−8870.
24. Singh, R., Wiseman, B., Deemagarn, T., Donald, L. J., Duckworth, H. W., Carpena, X., Fita, I., and Loewen, P. C. (2004) Catalase-peroxidases (KatG) exhibit NADH oxidase activity, *J. Biol. Chem. 279*, 43098−44106.
25. Wengenack, N. L., and Rusnak, F. (2001) Evidence for isoniazid-dependent free radical generation catalyzed by *Mycobacterium tuberculosis* KatG and the isoniazid-resistant mutant KatG(S315T), *Biochemistry 40*, 8990−8996.
26. Wei, C.-J., Lei, B., Musser, J. M., and Tu, S.-C. (2003) Isoniazid activation defects in recombinant *Mycobacterium tuberculosis* catalase-peroxidase (KatG) mutants evident in InhA inhibitor production, *Antimicrob. Agents Chemother. 47*, 670−675.
27. Sinha, B. K. (1983) Enzymatic activation of hydrazine derivatives. A spin-trapping study, *J. Biol. Chem. 258*, 796−801.
28. Wilming, M., and Johnsson, K. (1999) Spontaneous formation of the bioactive form of the tuberculosis drug isoniazid, *Angew. Chem., Int. Ed. Engl. 38*, 2588−2590.
29. Nguyen, M., Quemard, A., Broussy, S., Bernadou, J., and Meunier, B. (2002) Mn(III) pyrophosphate as an efficient tool for studying the mode of action of isoniazid on the InhA protein of *Mycobacterium tuberculosis*, *Antimicrob. Agents Chemother. 46*, 2137−2144.
30. Nguyen, M., Claparols, C., Bernadou, J., and Meunier, B. (2001) A fast and efficient metal-mediated oxidation of isoniazid and identification of isoniazid-NAD(H) adducts, *ChemBioChem 2*, 877−883.
31. Ghiladi, R. A., Cabelli, D. E., and Ortiz de Montellano, P. R. (2004) Superoxide reactivity of KatG: insights into isoniazid resistance pathways in TB, *J. Am. Chem. Soc. 126*, 4772−4773.
32. Wengenack, N. L., Hoard, H. M., and Rusnak, F. (1999) Isoniazid oxidation by *Mycobacterium tuberculosis* KatG: A role for superoxide which correlates with isoniazid susceptibility, *J. Am. Chem. Soc. 121*, 9748−9749.
33. Ghiladi, R. A., Medzihradszky, K. F., Rusnak, F. M., and Ortiz de Montellano, P. R. (2005) Correlation between isoniazid resistance and superoxide reactivity in *Mycobacterium tuberculosis* KatG, *J. Am. Chem. Soc. 127*, 13428−13442.
34. Gonzalez-Flecha, B., and Demple, B. (1997) Homeostatic regulation of intracellular hydrogen peroxide concentration in aerobically growing *Escherichia coli*, *J. Bacteriol. 179*, 382−388.
35. Ng, V. H., Cox, J. S., Sousa, A. O., MacMicking, J. D., and McKinney, J. D. (2004) Role of KatG catalase-peroxidase in mycobacterial pathogenesis: countering the phagocyte oxidative burst, *Mol. Microbiol. 52*, 1291−1302.
36. Bertrand, T., Eady, N. A. J., Jones, J. N., Jesmin, Nagy, J. M., Jamart-Gregoire, B., Raven, E. L., and Brown, K. A. (2004) Crystal structure of *Mycobacterium tuberculosis* catalase-peroxidase, *J. Biol. Chem. 279*, 38991−38999.
37. Zhao, X., Girotto, S., Yu, S., and Magliozzo, R. S. (2004) Evidence for radical formation at Tyr-353 in *Mycobacterium tuberculosis* catalase-peroxidase (KatG), *J. Biol. Chem. 279*, 7606−7612.
38. Otwinowski, Z., and Minor, W. (1997) in *Methods in Enzymology* (Carter, C. W., and Sweet, R. M., Eds.) pp 307−326, Academic Press, San Diego.
39. Vagin, A., and Teplyakov, A. (1997) MOLREP: an automated program for molecular replacement, *J. Appl. Crystallogr. 30*, 1022−1025.
40. Collaborative Computational Project (1994) The CCP4 suite: programs for protein crystallography, *Acta Crystallogr. D50*, 760−763.
41. Ioerger, T. R., Holton, T., Christopher, J. A., and Sacchettini, J. C. (1999) TEXTAL: a pattern recognition system for interpreting electron density maps, *Proc. Int. Conf. Intell. Syst. Mol. Biol.*, 130−137.
42. Brunger, A. T., Adams, P. D., Clore, G. M., DeLano, W. L., Gros, P., Grosse-Kunstleve, R. W., Jiang, J.-S., Kuszewski, J., Nilges, M., Pannu, N. S., Read, R. J., Rice, L. M., Simonson, T., and Warren, G. L. (1998) Crystallography & NMR system: A new software suite for macromolecular structure determination, *Acta Crystallogr. D54*, 905−921.
43. McRee, D. E. (1999) XtalView/Xfit−A versatile program for manipulating atomic coordinates and electron density, *J. Struct. Biol. 125*, 156−165.
44. Perrakis, A., Harkiolaki, M., Wilson, K. S., and Lamzin, V. S. (2001) ARP/wARP and molecular replacement, *Acta Crystallogr. D57*, 1445−1450.
45. Laskowski, R. A., MacArthur, M. W., Moss, D. S., and Thornton, J. M. (1993) PROCHECK: a program to check the stereochemical quality of protein structures, *J. Appl. Crystallogr. 26*, 283−291.
46. Magliozzo, R. S., and Marcinkeviciene, J. A. (1996) Evidence for isoniazid oxidation by oxyferrous mycobacterial catalase-peroxidase, *J. Am. Chem. Soc. 118*, 11303−11304.
47. Yokota, K., and Yamazaki, I. (1977) Analysis and computer simulation of aerobic oxidation of reduced nicotinamide adenine dinucleotide catalyzed by horseradish peroxidase, *Biochemistry 16*, 1913−1920.
48. Johnsson, K., Froland, W. A., and Schultz, P. G. (1997) Overexpression, purification, and characterization of the catalase-peroxidase KatG from *Mycobacterium tuberculosis*, *J. Biol. Chem. 272*, 2834−2840.
49. Ogura, Y. (1955) Catalase activity at high concentration of hydrogen peroxide, *Arch. Biochem. Biophys. 57*, 288−300.
50. Kapetanaki, S., Chouchane, S., Girotto, S., Yu, S., Magliozzo, R. S., and Schelvis, J. P. (2003) Conformational differences in *Mycobacterium tuberculosis* catalase-peroxidase KatG and its S315T mutant revealed by resonance Raman spectroscopy, *Biochemistry 42*, 3835−3845.
51. Carpena, X., Loprasert, S., Mongkolsuk, S., Switala, J., Loewen, P. C., and Fita, I. (2003) Catalase-peroxidase KatG of *Burkholderia pseudomallei* at 1.7Å resolution, *J. Mol. Biol. 327*, 475−489.
52. Deemagarn, T., Carpena, X., Singh, R., Wiseman, B., Fita, I., and Loewen, P. C. (2005) Structural characterization of the Ser324Thr variant of the catalase-peroxidase (KatG) from *Burkholderia pseudomallei*, *J. Mol. Biol. 345*, 21−28.
53. Pierattelli, R., Banci, L., Eady, N. A. J., Bodiguel, J., Jones, J. N., Moody, P. C. E., Raven, E. L., Jamart-Gregoire, B., and Brown, K. A. (2004) Enzyme-catalyzed mechanism of isoniazid activation in class I and class III peroxidases, *J. Biol. Chem. 279*, 39000−39009.
54. Kapetanaki, S. M., Chouchane, S., Yu, S., Zhao, X., Magliozzo, R. S., and Schelvis, J. P. (2005) *Mycobacterium tuberculosis* KatG(S315T) catalase-peroxidase retains all active site properties for proper catalytic function, *Biochemistry 44*, 243−252.
55. Hillar, A., and Loewen, P. C. (1995) Comparison of isoniazid oxidation catalyzed by bacterial catalase-peroxidases and horseradish peroxidase, *Arch. Biochem. Biophys. 323*, 438−446.
56. Kremer, M. L. (1970) Peroxidatic activity of catalase, *Biochim. Biophys. Acta 198*, 199−209.
57. Kusunose, E., Ichihara, K., Noda, Y., and Kusunose, M. (1976) Superoxide dismutase from *Mycobacterium tuberculosis*, *J. Biochem. (Tokyo) 80*, 1343−1352.
58. Zhang, Y., Lathigra, R., Garbe, T., Catty, D., and Young, D. (1991) Genetic analysis of superoxide dismutase, the 23 kilodalton antigen of *Mycobacterium tuberculosis*, *Mol. Microbiol. 5*, 381−391.
59. Musser, J. M., Kapur, V., Williams, D. L., Kreiswirth, B. N., van Soolingen, D., and van Embden, J. D. (1996) Characterization of the catalase-peroxidase gene (katG) and inhA locus in isoniazid-resistant and -susceptible strains of *Mycobacterium tuberculosis* by automated DNA sequencing: restricted array of mutations associated with drug resistance, *J. Infect. Dis. 173*, 196−202.
60. Victor, T. C., Pretorius, G. S., Felix, J. V., Jordaan, A. M., van Helden, P. D., and Eisenach, K. D. (1996) katG mutations in isoniazid-resistant strains of *Mycobacterium tuberculosis* are not infrequent, *Antimicrob. Agents Chemother. 40*, 1572.
61. Heym, B., Alzari, P. M., Honore, N., and Cole, S. T. (1995) Missense mutations in the catalase-peroxidase gene, katG, are associated with isoniazid resistance in *Mycobacterium tuberculosis*, *Mol. Microbiol. 15*, 235−245.
62. Wengenack, N. L., and Rusnak, F. (2001) Evidence for isoniazid-dependent free radical generation catalyzed by *Mycobacterium tuberculosis* KatG and the isoniazid-resistant mutant KatG(S315T), *Biochemistry 40*, 8990−8996.
63. Ghiladi, R. A., Knudsen, G. M., Medzihradszky, K. F., and de Montellano, P. R. O. (2005) The Met-Tyr-Trp cross-link in

Mycobacterium tuberculosis catalase-peroxidase (KatG), *J. Biol. Chem. 280*, 22651−22663.
64. Chouchane, S., Girotto, S., Kapetanaki, S., Schelvis, J. P., Yu, S., and Magliozzo, R. S. (2003) Analysis of heme structural heterogeneity in *Mycobacterium tuberculosis* catalase-peroxidase (KatG), *J. Biol. Chem. 278*, 8154−8162.
65. Christopher, J. A., Swanson, R., and Baldwin, T. O. (1996) Algorithms for finding the axis of a helix: Fast rotational and parametric least-squares methods, *Comput. Chem. 20*, 339−345.

BI051967O